High-Resolution Raman Spectroscopy Study of Phonon Modes in $LiBH_4$ and $LiBD_4$

A.-M. Racu* and J. Schoenes

Institute of Condensed Matter Physics, Technical University Braunschweig, Mendelssohnstrasse 3, D-38106 Braunschweig, Germany

Z. Lodziana, A. Borgschulte, and A. Züttel

EMPA, Materials Science and Technology, Department of Mobility, Environment, and Energy, Div. Hydrogen and Energy, Überlandstr. 129, 8600 Dübendorf, Switzerland

Received: April 7, 2008; Revised Manuscript Received: July 15, 2008

We have performed micro Raman measurements on $LiBH_4$ and $LiBD_4$ powders for temperatures between 5 and 300 K. At the lowest temperature, the peak energies agree very well with the results of a calculation within the density functional theory for the orthorhombic structure. The spectra are dominated by three separated bands: the external modes, the internal bending, and the internal stretching vibrations. Internal refers to vibrations within the BH_4 tetrahedrons, whereas external modes imply motions of Li and BH_4. The temperature dependence of the observed phonons corroborates the strong anharmonicity of the system. Due to the anharmonicity, Fermi resonances occur between the first order stretching modes and the second order bending modes of $LiBH_4$. Moreover, the linewidths of the observed modes in $LiBH_4$ have an Arrhenius-like component, with activation energies ranging from 250 to 500 K.

1. Introduction

The complex hydrides are at the moment among the most promising systems for hydrogen storage.[1] Theoretically, $LiBH_4$ can store 18 mass % hydrogen, which is substantially larger than the DOE roadmap value for 2015. Numerous studies of this system revealed high decomposition temperatures, suggesting strong hydrogen bonds.[2] With increasing temperature, $LiBH_4$ undergoes first a phase transition from an orthorhombic to a hexagonal structure at about 380 K and then melts at about 540 K. At present the high decomposition temperature is a strong impediment for the technical use of LiBH4 in mobile applications. Therefore, basic research is needed to understand the mechanism of thermal desorption and absorption[3] allowing then either to modify the bond strengths or to find new reliable hydrogen storage systems. Züttel et al.[3] found for the tetrahydroborates MBH_4 and tetrahydroaluminates $MAlH_4$ that the decomposition temperature is linearly related to the Pauling electronegativity of the alkali metal M as well as to the electronegativity of B and Al. Orimo et al.[4] pointed out the correlation between the electronegativity of the cation and the frequency of the bending and stretching modes of hydrogen in the BH_4 complex. A concept to reduce the desorption temperature foresees a destabilization of metal hydrides by embedding the hydrides in high surface area materials[5] which would manifest itself in a softening of phonon frequencies.

While the sole electron of hydrogen presents a small scattering cross section for X-rays and renders structure determinations quite difficult, the light mass of hydrogen leads to large vibration frequencies making Raman spectroscopy, in principle, a particularly powerful technique to study the crystallographic structure and the bond strengths in hydrides.[6,7] In addition, the exchange of hydrogen with deuterium can lead to large shifts, helping one to identify the vibrations. Yet, limited resolution, thermal broadenings, and anharmonicities may severely reduce the number of identifiable lines, making assignments very speculative. Thus, to date, only 13 out of 36 expected single modes have been identified in the low-temperature phase. First Raman studies on $LiBH_4$ in 1971 have been performed by Harvey and McQuaker,[8] who observed six lines, five of which having been assigned within the *Pcmn* space group derived prior from X-ray scattering[9] to internal BH_4 vibrations and one to a second overtone of a librational mode. Later in 2002, Gomes et al.[10] assigned 13 single modes and 4 combination bands within the space group *Pnma*. Only 3 out of the expected 18 lines could be observed in the energy range of the external Li−BH_4 vibrations, which are particularly sensitive to the crystallographic structure and anharmonicities. In 2004, Miwa et al.[11] reported a first principle calculation of the phonons and the dielectric function and noted the observation of 3 Raman lines near 1300 and 2300 cm^{-1}. In the present paper, we present a comprehensive Raman study of the crystallographic structure and the bonds of the low temperature phase of $LiBH_4$ and $LiBD_4$. By cooling the samples to liquid-helium temperature and using a high resolution Raman spectrometer, we can identify 27 single modes. The comparison of the experimental results for the two hydrogen isotopes among each other and with the results of a new first principle calculation allows reliable assignments of all Raman peaks to vibration modes. Plotting the theoretical against the experimental frequencies, the average agreement of the frequencies is better than 1 and 4% for the external and internal vibrations, respectively. The temperature dependence of the vibration frequencies, linewidths, and intensities shows some remarkable behaviors pointing to nonharmonic vibrations, thermally activated relaxation processes, and a possible precursor of the phase transition at 380 K.

2. Theory

The structure and the normal-mode analysis of $LiBH_4$ were calculated within the density functional theory (DFT).[12] Ele-

* To whom correspondence should be addressed. E-mail: a.racu@tu-bs.de.

10.1021/jp803005f CCC: $40.75
Published on Web 09/11/2008

ments were represented by the projected augmented plane-wave potentials (PAW)[13,14] with electronic configuration $1s^2 2s^1$ for Li, $2s^2 2p^1$ for B and $1s^1$ for H. For Li the 1s electrons were considered as the valence electrons, since the lithium in $LiBH_4$ is always present as Li^+. The calculations were carried out within the generalized gradient approximation (GGA) using the PW91 exchange correlation functional[15] and the kinetic energies cutoff of 400 eV. The wave functions were sampled according to the Monkhorst-Pack scheme with a k-points mesh of ~0.05 $Å^{-1}$. This procedure resulted in the ground-state energy convergence of less than 0.01 eV/formula unit, which is considered as sufficient for the present purposes. The lattice dynamics was determined with the so-called direct method.[16−18] The supercell containing 96 atoms was constructed from the primitive *Pnma* unit cell. The Hellman-Feynman forces were calculated by sets of finite displacements (±0.02 Å) of the symmetry nonequivalent atoms. The resulting forces were transformed into sets of force constants to assembly a dynamical matrix.

In the present approach, effective charges were not taken into account, which gives a potential source of errors. We have checked that effective charges[11] introduced to the system do not affect our results. In the present studies we focus on Raman active optical modes that are not affected by macroscopic electric fields.

3. Experimental Section

The $LiBH_4$ (Sigma Aldrich, purity 95%) and $LiBD_4$ (CatChem, purity 98%) samples have been filled into the sample chamber of the cryostat (Konti, type Micro, CryoVac) in Ar atmosphere. Raman spectra have been recorded using a commercial micro-Raman spectrometer (Jobin Yvon LabRam HR), adapted to the cryostat. The excitation radiation is the 532 nm wavelength line of a diode-pumped Nd:YAG laser of 50 mW. The light beam is focused on an area of a few μm^2. The resolution is about 2.3 cm^{-1}. The temperature resolved measurements have been performed during heating from 5 to 300 K.

4. Results and Discussion

The analysis of the factor group for the orthorhombic *Pnma* structure reveals a total number of 36 Raman active modes

$$\Gamma = 11A_g + 7B_{1g} + 11B_{2g} + 7B_{3g} \quad (1)$$

18 of which are external vibrations (the BH_4^- entity moves against Li^+), and the other 18 are internal vibrations (originating from the bending and stretching motions of the free BH_4 tetrahedrons). The vibrations of the free BH_4 units split in a crystal, due to the correlation field effects. Usually, these effects are small and do not give measurable splittings at room temperature. Up to date, the assignment of the observed Raman modes in $LiBH_4$, $LiBD_4$,[8,10] and compounds with other anions (Na, K, and Cs) follow the scheme proposed by Harvey and McQuaker,[8] who considered the 9 normal vibrations of the BH_4^- ion. We are now in the position to classify the lines following the factor group analysis (eq 1). Nevertheless, to allow a comparison with the older data, we also include the notation which neglects the effect of the crystal field.

Figure 1 shows an overview of the Raman spectra of $LiBH_4$ and $LiBD_4$ at 5 K. One can delimitate 3 regions: the modes below 500 cm^{-1} are mainly due to translational and librational motions of the Li and BH_4 frameworks. Between 1000 and 1400 cm^{-1} in $LiBH_4$ (800 and 1000 cm^{-1} in $LiBD_4$) are the bond-bending vibrations of BH_4 (BD_4). The very strong lines situated at higher frequencies are the bond-stretching vibrations. The

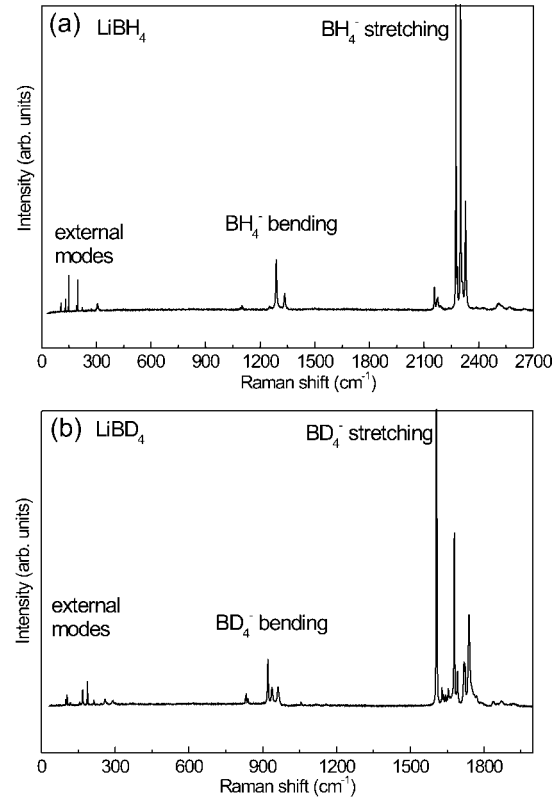

Figure 1. Raman spectra of (a) $LiBH_4$ and (b) $LiBD_4$ at 5 K. The external modes and the bending and stretching internal modes will be discussed separately.

frequencies of the stretching modes are approximately twice the frequencies of the bending modes. Fermi resonances occur between the stretching modes and the first overtones of the bending modes. Due to the Fermi resonances, the intensities of the second order lines are higher than the intensities of the fundamental lines, and their frequencies are shifted.[19] This makes an empirical mode assignment very difficult and stresses the necessity to compare the measurements to calculations. Table 1 presents the frequencies of the Raman modes at room temperature and at 5 K, together with the calculated values for $LiBH_4$ and $LiBD_4$. In the following, we divide our discussion in internal and external lattice vibrations.

4.1. External Modes. The measurement on a powder sample does not allow a clear assignment of the Raman modes to the symmetry species. Indeed, the intensity of the Raman lines is the same in different measuring geometries (polarizations), implying a random orientation of the crystallites. Therefore, the mode assignment is the result of a minutious comparison with the theoretical values, as well as the analysis of their behavior as a function of temperature. A collection of Raman spectra measured at different temperatures in the region of the external vibrations is presented in Figure 2. The insets show the experimental vs calculated frequencies. The encouraging agreement (slope of the line-fits is 1) supports our assignment of the Raman modes. To the best of our knowledge, the external Raman modes have not been assigned to the symmetry species, yet.

Figure 3 shows the temperature dependence of the normalized frequency, line width, and intensity for several external modes of $LiBH_4$ and $LiBD_4$. The other external modes (not shown in Figure 3) display temperature dependencies which lie within the B_{2g} mode at 306.9 cm^{-1} and the A_g mode at 198 cm^{-1}.

There is one Raman mode which displays an extraordinary behavior: the B_{3g} mode at 148.8 cm^{-1} in $LiBH_4$ which

TABLE 1: Experimental Raman Frequencies (cm^{-1}) of $LiBH_4$ and $LiBD_4$ at Room Temperature and at 5 K Compared to the Calculated Values

	$LiBH_4$			$LiBD_4$			ratio (theory)	ratio (5 K)
mode	300 K	5 K	theory	300 K	5 K	theory	ω_H/ω_D	ω_H/ω_D
				external modes				
A_g	96	105.6	107	90	98.7	84.13	1.27	1.06
B_{1g}			125.6	127	118.03	112.13	1.12	
B_{3g}	119	130.5	136.6			119.2	1.14	
B_{3g}	150	148.8	155.3	106	104.1	100.43	1.54	1.42
B_{2g}		192.4	199.6	166.8	167.7	175.8	1.13	1.14
B_{1g}			212		155.6	157.2	1.34	
A_g	191.6	198	213.3	178.03	187.3	194.5	1.09	1.05
A_g		223.5	263.3			246.3	1.06	
B_{3g}		257	274.6	240	242.5	249.5	1.10	1.05
B_{2g}		272.7	276.3	201	213.5	241.9	1.14	1.27
B_{1g}			290	242.8	258.6	263.16	1.10	
B_{2g}	287.8	306.9	292.3	263.6	290.18	269.5	1.08	1.05
A_g			350.3			331	1.05	
B_{2g}			392			366.2	1.07	
B_{3g}			439			318.23	1.37	
B_{2g}			455.3			401.93	1.13	
B_{1g}			459.6			340.76	1.34	
A_g			483			380.3	1.26	
				internal bending				
ν_4 (A_g)	1098	1090	1062.6	833	829	805.5	1.31	1.31
ν_4 (B_{2g})		1099	1064.66			805.7	1.32	
ν_4'' (B_{1g})		1105	1070.3		832	807.7	1.32	1.32
ν_4'' (B_{3g})			1070.3		839	809.13	1.32	
ν_4' (A_g)	1240	1252	1235.3		937	919.7	1.34	1.33
ν_4' (B_{2g})			1242.3			920.6	1.34	
ν_2'' (B_{1g})	1290	1288	1260	923	921	897.43	1.40	1.39
ν_2'' (B_{3g})			1265.3			901.1	1.40	
ν_2 (A_g)	1320	1334	1311.6	947	961	938.6	1.39	1.38
ν_2 (B_{2g})			1315.6			940.2	1.39	
				internal stretching				
ν_3 (A_g)	2273	2273	2329	1680	1678	1758.6	1.32	1.35
ν_3 (B_{2g})		2282	2329		1691	1768.6	1.31	1.34
ν_1 (A_g)	2298	2299	2371.6	1607	1606	1649.56	1.43	1.43
ν_1 (B_{2g})		2309	2384.6		1609	1652.16	1.44	1.43
ν_3'' (B_{1g})			2387.6	1720	1717	1772.8	1.34	
ν_3'' (B_{3g})			2389.3		1721	1774	1.34	
ν_3' (A_g)	2319	2326	2414	1738	1739	1794.7	1.34	1.33
ν_3' (B_{2g})			2427.3		1751	1801.9	1.34	

corresponds to the B_{3g} mode at 104.1 cm^{-1} in $LiBD_4$. It softens by a factor of 1.02 when the temperature decreases from room temperature to 5 K. In $LiBD_4$ there is a similar mode (not shown in Figure 3), the B_{1g} at 118.03 cm^{-1}. This mode is not visible in $LiBH_4$. The line width of the B_{3g} mode increases by a factor of 11 for $LiBH_4$ and 5 for $LiBD_4$, between 5 and 200 K, while a line broadening by a factor of about 4 is observed for most other modes (black symbols in the middle panel of Figure 3). Moreover, the normalized intensity of the peculiar B_{3g} mode drops more than all other modes in both $LiBH_4$ and $LiBD_4$. The peculiarity of this mode is encountered by an anomalously large isotope displacement (calculated ratio 1.54, measured 1.42). This can be understood since the frequency of a mode includes not directly the masses of the vibrating atoms but the reduced masses and the moments of inertia, together with lattice force constants. The moments of inertia become important when the vibration implies rotating units, which is the case of our peculiar B_{3g} mode. Indeed, animations of this B_{3g} mode for $LiBH_4$ and $LiBD_4$ reveal rotations of the BH_4 tetrahedrons (see Figure 4).

4.2. Internal Modes. The internal modes of $LiBH_4$ originate from the bond-bending and -stretching vibrations of the free BH_4 tetrahedrons. These vibrations split due to the crystal surrounding in the so-called correlation field.

The bending modes of $LiBH_4$ and $LiBD_4$ are presented in Figure 5, panels a and b, respectively. This region is dominated by symmetric (ν_2) and asymmetric (ν_4) vibrations. The insets show the experimental (at 5 K) vs theoretical data which were successfully fitted by a line with a slope of 1.03.

Figure 6, panels a and b, presents the stretching modes of $LiBH_4$ and $LiBD_4$. The symmetric stretching mode ν_1 which is situated between ν_3 and ν_3' in $LiBH_4$ shifts below $2\nu_4$ and $2\nu_4''$ in $LiBD_4$ and uncovers the mode ν_3''.

In addition to the external modes, Table 1 collects the frequencies of the measured and calculated internal modes of $LiBH_4$ and $LiBD_4$. As mentioned before, we use the scheme proposed by Harvey and McQuaker[8] and for the first time, the symmetry notations after the crystal field has split the free ion states into A_g, B_{1g}, B_{2g}, and B_{3g} modes. The isotope exchange ratios are consistent with the results obtained by Renaudin et al.[20] for MBH_4 with M (Na, K, Rb, and Cs): the ν_1 modes have the highest shift (a factor of 1.43), followed by the ν_2', ν_2, and ν_3 with factors of 1.39, 1.38, and 1.35, respectively. Finally, the ν_4, ν_4', and ν_4'' modes display isotopic ratios of 1.31, 1.33,

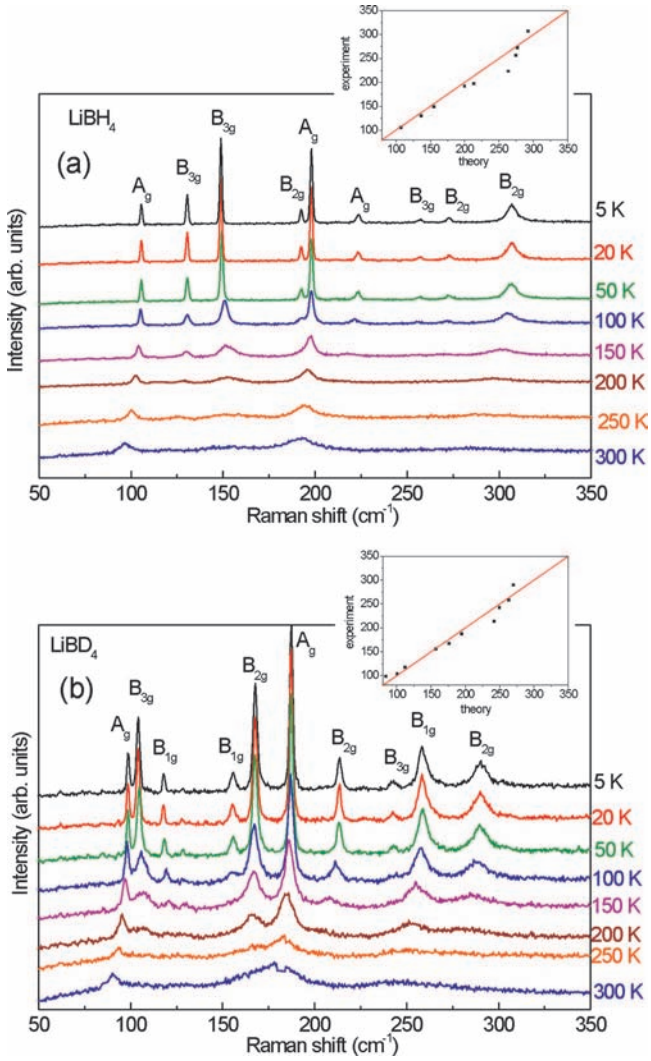

Figure 2. Raman spectra of (a) $LiBH_4$ and (b) $LiBD_4$ at different temperatures, in the region of the external vibrations. The insets present the experimental vs theory frequencies fitted by a line with a slope of 1.

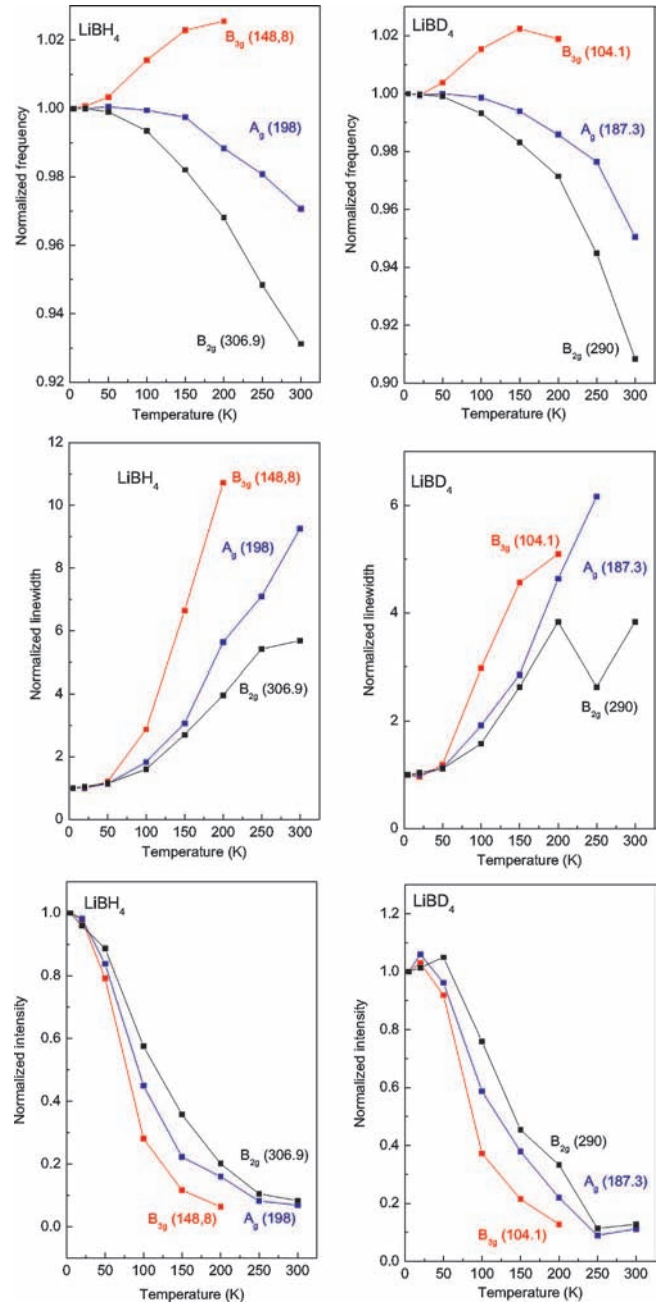

Figure 3. Temperature dependence of the frequency, line width, and intensity normalized to the value at 5 K for several external Raman modes of $LiBH_4$ (left) and $LiBD_4$ (right). The values in brackets represent the positions of the lines (in cm^{-1}) at 5 K.

and 1.32, respectively. Our temperature dependent measurements from 5 to 300 K are in good agreement with the anharmonicity and the presence of Fermi resonances, inferred by several authors from room temperature Raman and infrared measurements and calculations.[19] The anharmonicity is reflected by the temperature dependence of the frequencies and linewidths of the observed Raman modes, while Fermi resonances are seen for the overtones of ν_4 and ν_4''. We assign the peak at 1240 cm^{-1} (room temperature) to the ν_4' mode, in contrast to the existent literature data, which attributed it to the second overtone of the librational mode.[10] In $LiBD_4$, ν_4' lies between ν_2 and ν_2' due to the small isotope exchange ratio for ν_4', as mentioned above.

We observe in the insets of Figure 6 that the calculated frequencies deviate by a factor of 0.971 and 0.965 from the experimental values for hydride and deuteride, respectively. In contrast to the external and bending modes, we observe some scattering of the data points from a straight line. Some theoretical frequencies are too low (points above the straight line in the insets of Figure 6) and others are too high (points below the straight line). The largest deviations are about 10%.

These deviations could be due to the presence of charges inside the BH_4 tetrahedrons. The Al−H bonds of the related compound $NaAlH_4$ were characterized by Ozolins et al.[21] as polar covalent. Aguayo et al.[22] argued that $NaAlH_4$ is better described as mixed ionic, i.e., $Na^+Al^{3+}H_4^-$ than the usual covalent picture. The situation in $LiBH_4$ is different, since the Pauling electronegativity of H (2.2) is very close to that of B (2.04). Nevertheless, the B−H bonds may have a very small polarity which can affect the frequencies of the stretching modes.

Reference 20 showed that in MBD_4 with M (Na, K, Rb, and Cs) the Badger's rule is fulfilled at room temperature, i.e., there is a linear relation between B-D bond lengths d and the Raman shifts of the totally symmetric mode ν_1 expressed as $\nu_1^{-2/3} = \alpha d(\mathrm{B-D}) - \beta$, where α and β are constants. Extrapolating the curve in ref 20 and using the frequency of our measured ν_1 mode of $LiBD_4$, we deduce a B−D bond length of about 1.185 Å. This agrees with the value of 1.184 Å derived recently[23]

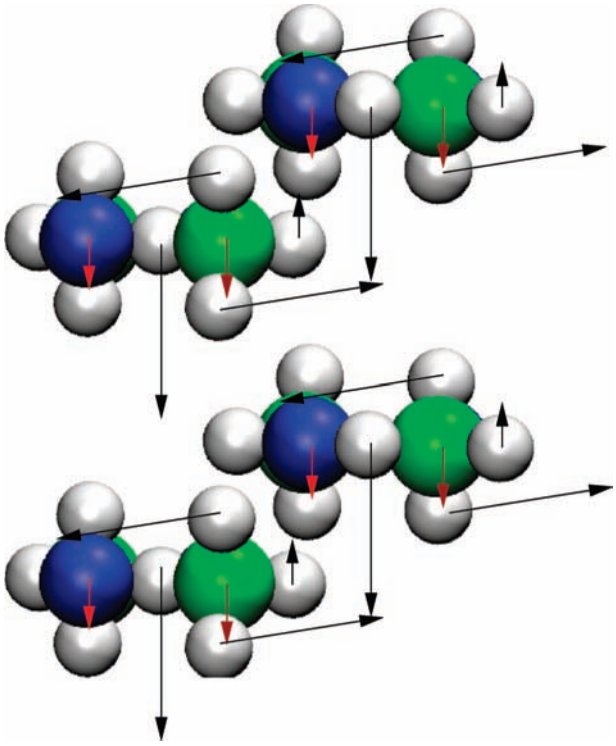

Figure 4. Illustration of the B_{3g} mode at 148.8 cm^{-1} in $LiBH_4$. The z axis is horizontal from right to left, and the y axis is vertical from bottom to top. Green (light gray) big circles represent the B atoms, surrounded by the H atoms (light gray small circles). Blue (dark gray) big circles are the Li atoms. For simplicity, we represented only the rotations of the BH_4 tetrahedrons situated in the front plane by counterclockwise oriented arrows. The BH_4 tetrahedrons from the back plane rotate inversely.

from neutron diffraction experiments for the B−H1 bond and disagrees with the value of 1.04 Å derived previously from synchrotron X-ray diffraction.[24] In the latter case, it was suggested that the BH_4 tetrahedrons are severely distorted with B−H2 and B−H3 bond lengths of 1.25 and 1.28 Å, respectively.[24] Our data clearly favor the less distorted model of Hartman et al.[23] with bond lengths ranging from 1.184 Å (B−H1 and B−H3) to 1.217 Å (B−H2).

In the last part of this paper, we analyze quantitatively the temperature dependence of the linewidths of the internal and external modes of $LiBH_4$. Generally, the line width of a Raman mode gives valuable information about possible phonon relaxation mechanisms. The most simple process is the decay of an optical phonon into two acoustic modes.[25] In this case, the line-broadening for one particular mode can be written as

$$\Gamma_P(T) = \Gamma_0\left(1 + \frac{2}{e^y - 1}\right) \quad (2)$$

where Γ_0 is the harmonic line width, $y = \hbar\omega_0/k_BT$ and ω_0 is the harmonic frequency. This type of relaxation process is particularly important for the external modes, for which the energy is lower than k_BT in the range of temperatures studied.

The line width at temperature T can be written as a sum of the broadening due to phonon−phonon interactions described by eq 2 and a residual term summarizing other types of phonon decay.

$$\Gamma(T) = \Gamma_P(T) + \Gamma_R(T) \quad (3)$$

In the case of the internal and external modes of $LiBH_4$, the residual term follows an exponential relation of the form

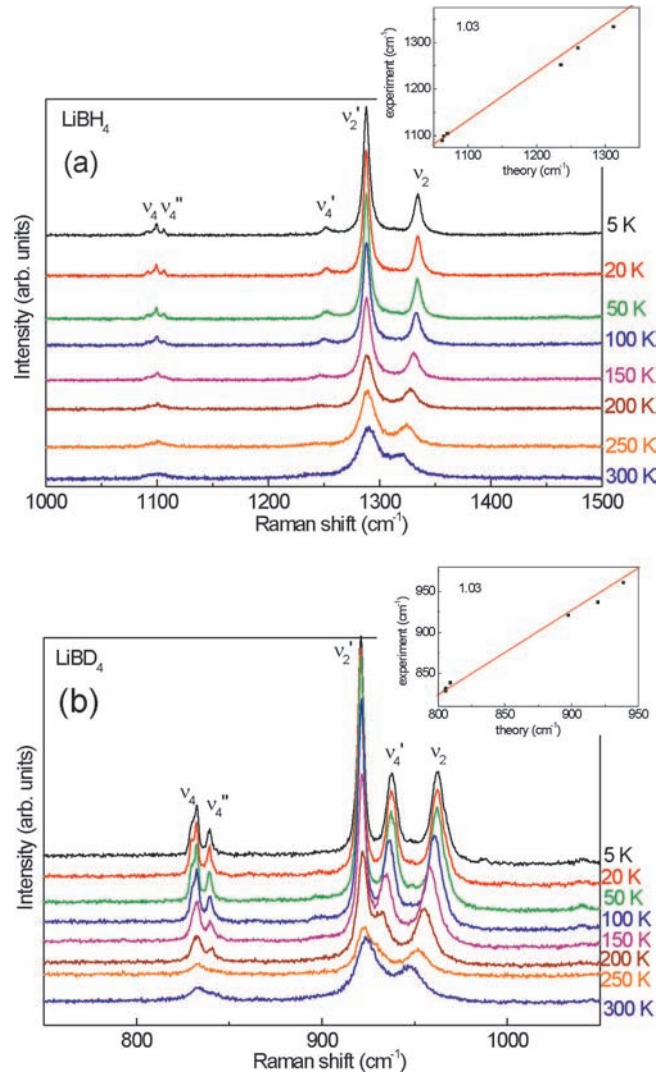

Figure 5. The internal bending modes of (a) $LiBH_4$ and (b) $LiBD_4$ at different temperatures. The insets present the experimental vs theory frequencies fitted by a line with a slope of 1.03.

$$\Gamma_R(T) = Ae^{-U/k_BT} \quad (4)$$

where A is a constant and U is an activation energy. Such an activated behavior of linewidths as a function of temperature has been observed for example in $Ni(H_2O)_6$ SiF_6 and was discussed in terms of anharmonic interactions.[26] Anharmonicity in the potential function can contribute to the temperature dependence of a vibrational state in two ways: (i) thermal expansion, leading to a frequency shift but not to line broadening, and (ii) thermal fluctuations, inducing a coupling between different vibrations. This leads to both frequency shift and line broadening. If the energy U of the phonon which scatters the excited vibrational state is in the range of k_BT at moderate temperatures, it has been shown that the line broadening has an Arrhenius-type temperature dependence like that given by eq 4.

We have analyzed the temperature dependence of the linewidths for the largest external and internal Raman modes observed experimentally in $LiBH_4$. As typical examples, Figure 7 shows Arrhenius plots ($\ln(\Gamma_R/\Gamma_0)$ versus $1/T$) of the linewidths for the three external modes presented in Figure 3. The data points have been fitted by straight lines using two parameters: the activation energy in Kelvin U/k_B given by the slope of the lines, and the constant A. Except for the lowest A_g mode, the

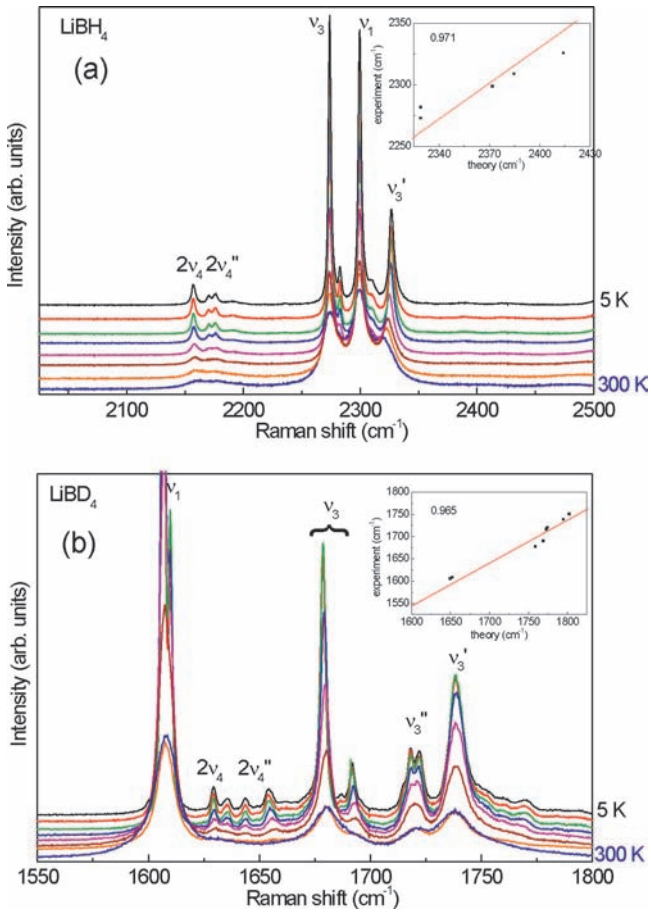

Figure 6. Internal stretching modes of (a) $LiBH_4$ and (b) $LiBD_4$ at different temperatures. The insets present the experimental vs theory frequencies fitted by lines with slopes of 0.971 and 0.965 for $LiBH_4$ and $LiBD_4$, respectively.

11 analyzed internal and external modes give good fits using activation energies lying between 250 and 500 K. Our Raman measurements as well as inelastic neutron spectra[23,27] show in this energy range high density of phonon states, supplying the necessary scattering channels.[26]

We have pointed out in section 4 that the B_{3g} mode at 148.8 cm^{-1} has a peculiar behavior concerning the temperature dependence of the frequency, line width, and intensity as well as an anomalously large isotope effect. In addition, Figure 7 suggests a large value of the prefactor of eq 4, compared to all other modes. This indicates that this B_{3g} mode is mostly affected by anharmonic effects.

Recently it was shown that the structural change at 380 K is related to simultaneous rotations of the BH_4 molecular units.[28] Reorientations of these groups in the (*b*, *c*) crystal plane of the low temperature phase lead to breaking of the *Pnma* symmetry and to transition to $P6_3mc$ phase. As already shown in Figure 4, the B_{3g} mode is a low frequency vibration which consists of synchronous in phase rotations of BH_4 groups within atomic (*b*, *c*) planes and antiphase rotations between planes along *a*. This relates it to the structural phase transition. As the volume change of the unit cell is related to the phase transition, the B_{3g} mode couples to another phonon form the Brillouin zone boundary resulting in strong anharmonic effects.

5. Summary

We have studied Raman spectra of $LiBH_4$ and $LiBD_4$ as a function of temperature, from 5 to 300 K. For the first time, the external and internal modes have been assigned to the A_g, B_{1g}, B_{2g}, and B_{3g} symmetry species, according to the results of a calculation within the DFT. The results of this study can be used as an appropriate set of input data for sophisticated hydrogen−deuterium exchange measurements.[29] In the region of the external vibrations, there is one peculiar B_{3g} mode at 148.8 cm^{-1} which is proposed to be related to the orthorhombic to hexagonal phase transition. From an Arrhenius-fit of the residual linewidths of the external and internal Raman modes, we deduce activation energies ranging from 250 to 500 K, pointing to strong anharmonic coupling between different vibrations.

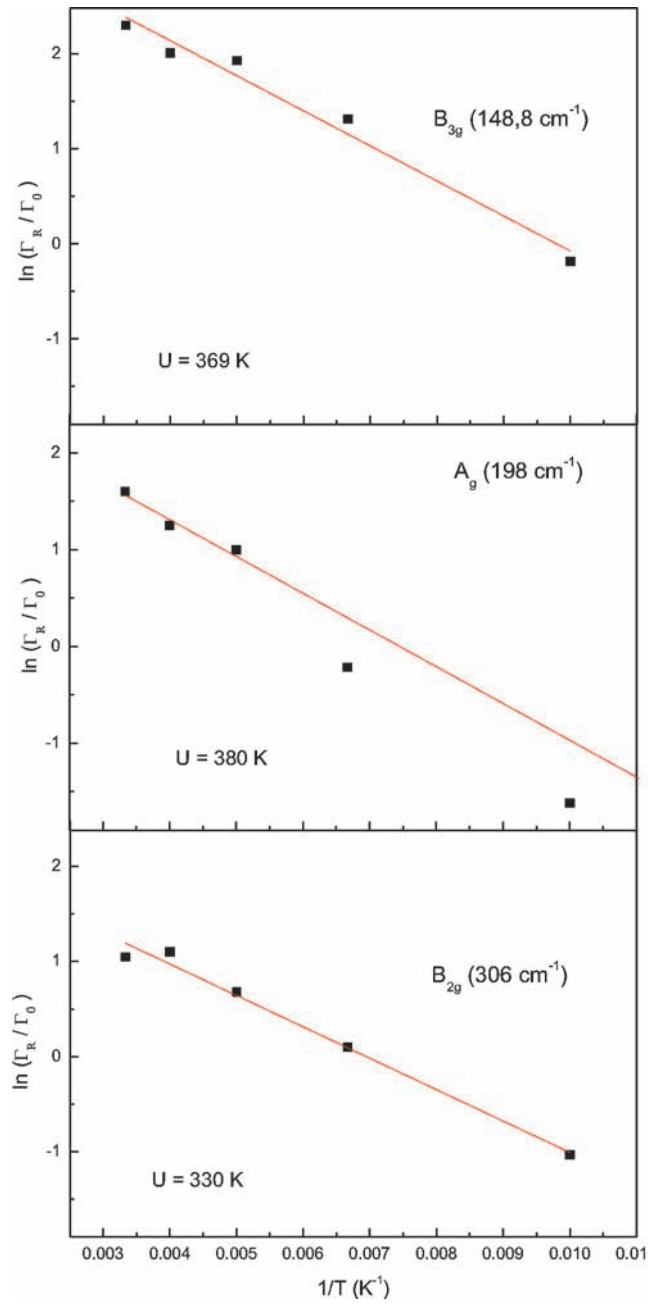

Figure 7. Arrhenius-plot of Γ_A for several internal Raman modes of $LiBH_4$.

Acknowledgment. The CPU time allocation at Swiss Supercomputer Center (CSCS, Manno) is kindly acknowledged.

References and Notes

(1) Schlapbach, L.; Züttel, A. *Nature* **2001**, *414*, 353.

(2) Orimo, S.; Nakamori, Y.; Kitahara, G.; Miwa, K.; Ohba, N.; Towata, S.; Züttel, A. *J. Alloys Comp.* **2005**, *404*, 427.
(3) Züttel, A.; Borgschulte, A.; Orimo, S. *Scr. Mater.* **2007**, *56*, 823.
(4) Orimo, S.; Nakamori, Y.; Züttel, A. *Mater. Sci. Eng., B* **2004**, *108*, 51.
(5) Vajo, J. J.; Olson, G. L. *Scr. Mater.* **2007**, *56*, 829.
(6) Kierey, H.; Rode, M.; Jacob, A.; Borgschulte, A.; Schoenes, J. *Phys. Rev. B* **2001**, *63*, 134109.
(7) Carsteanu, A.-M.; Rode, M.; Zur, D.; Borgschulte, A.; Schröter, H.; Schoenes, J. *Phys. Rev. B* **2004**, *69*, 134102.
(8) Harvey, K. B.; McQuaker, N. R. *Can. J. Chem.* **1971**, *49*, 3282.
(9) Harris, P. M.; Meibohm, E. P. *J. Am. Chem. Soc.* **1947**, *69*, 1231.
(10) Gomes, S.; Hagemann, H.; Yvon, K. *J. Alloys Comp.* **2002**, *346*, 206.
(11) Miwa, K.; Ohba, N.; Towata, S.; Nakamori, Y.; Orimo, S. *Phys. Rev. B* **2004**, *69*, 245120.
(12) Kresse, G.; Furthmüller, J. *Comput. Mater. Sci.* **1996**, *6*, 15.
(13) Blöchl, P. E. *Phys. Rev. B* **1994**, *50*, 17953.
(14) Kresse, G.; Joubert, D. *Phys. Rev. B* **1999**, *59*, 1758.
(15) Perdew, J. P.; Chevary, J. A.; Vosko, S. H.; Jackson, K. A.; Pederson, M. R.; Singh, D. J.; Fiolhais, C. *Phys. Rev. B.* **1992**, *46*, 6671.
(16) Parlinski, K.; Li, Z-.Q.; Kawazoe, Y. *Phys. Rev. Lett.* **1997**, *78*, 4063.
(17) Lodziana, Z.; Vegge, T. *Phys. Rev. Lett.* **2004**, *93*, 145501.
(18) Lodziana, Z.; Parlinski, K. *Phys. Rev. B* **2003**, *67*, 174106.
(19) Carbonniére, P.; Hagemann, H. *J. Phys. Chem. A* **2007**, *110*, 9927.
(20) Renaudin, G.; Gomes, S.; Hagemann, H.; Keller, L.; Yvon, K. *J. Alloys Comp.* **2004**, *375*, 98.
(21) Ozolins, V.; Mazjoub, E. H.; Udovic, T. J. *J. Alloys Comp.* **2004**, *375*, 1.
(22) Aguayo, A.; Singh, D. J. *Phys. Rev. B* **2004**, *69*, 155103.
(23) Hartman, M. R.; Rush, J. J.; Udovic, T. J.; Bowman, R. C., Jr.; Hwang, S.-J. *J. Solid State Chem.* **2007**, *180*, 1298.
(24) Soulié, J.-Ph.; Renaudin, G.; Cerny, R.; Yvon, K. *J. Alloys Comp.* **2002**, *346*, 200.
(25) Klemens, P. G. *Phys. Rev. B* **1975**, *11*, 3206.
(26) Jenkins, T. E.; Lewis, J. *J. Raman Spectrosc.* **1981**, *11*, 1.
(27) Tomkinson, J.; Waddington, T. C. *J. Chem. Soc. Faraday Trans 2* **1976**, *72*, 528.
(28) Filinchuk, Y.; Chernyschov, D.; Cerny, R. Submitted to *J. Phys. Chem. B.*
(29) Borgschulte, A.; Züttel, A.; Hug, P.; Racu, A.-M.; Schoenes, J. *J. Phys. Chem. A* **2008**, *112*, 4749.

JP803005F